Diabetic Retinopathy Prediction Using Machine Learning

Saman Naaz , Rutuja Biradar , Sakshi Jaybhaye , Dr. Vijay R Tripathi.

***Abstract*— Traditional classification algorithms struggle to categorize hypertensive retinopathy (HR) lesions correctly because they lack obvious characteristics. A regional IoT-enabled fed- erated learning-based HR categorization approach (IoT-FHR) incorporating global and local attributes is suggested as a solution to this issue. The local feature arterial and venous nicking (AVN) classification model is fused with the overall IoT-FHR classifica- tion model to enhance the effect of the classification of IoT-FHR. The AVN classification model's local lesion characteristics and the IoT-FHR classification model's global lesion characteristics were combined using feature mean. After that, the results of the global IoT-FHR classification model are averaged with the results of the local AVN classification model. An easy neural network receives its input from the final outcome. The probability value of IoT-FHR in the fundus image is output by the sigmoid classifier after the neural network's two fully connected and one dropout layer. The AVN classification makes a new kind of intersection detection algorithm suggestion. To determine the intersection points, the algorithm applies a logical AND operation to the classified arteries and veins. It takes HR fundus pictures and extracts AVN image blocks using the region of interest extraction approach. The accuracy, sensitivity, and specificity of the suggested fusion model are 93.50%, 69.83%, and 98.33%, respectively, when tested on a private dataset. It is clear from the experiments and results that the suggested model leads the currently used methods when the single-stage classification model is compared with them.**

***Index Terms*— Biomedical image, federated learning, fundus images, hypertensive retinopathy (HR), Internet of Things (IoT).**

Manuscript received 30 June 2022; revised 23 August 2022 and 27 September 2022; accepted 30 September 2022. Date of publication 2 November 2022; date of current version 2 August 2023. *(Corresponding author: Mohammad Shabaz.)*

Mukesh Soni is with the Department of CSE, University Centre for Research and Development, Chandigarh University, Mohali, Punjab 140413, India (e-mail: mukesh.t1712@cumail.in).
Nikhil Kumar Singh is with the Department of Computer Science and Engineering, Maulana Azad National Institute of Technology, Bhopal, Madhya Pradesh 462007, India (e-mail: nikhilsinghmanit@gmail.com).
Pranjit Das is with the Department of CSE, Koneru Lakshmaiah Education Foundation (K L University), Vaddeswaram 522302, India (e-mail: 91pranjitdas@gmail.com).
Mohammad Shabaz is with the Model Institute of Engineering and Technology, Jammu, Jammu and Kashmir 181122, India (e-mail: mohammad.shabaz@amu.edu.et).
Piyush Kumar Shukla is with the Department of Computer Science and Engineering, University Institute of Technology, Rajiv Gandhi Proudyogiki Vishwavidyalaya (Technological University of Madhya Pradesh), Bhopal, Madhya Pradesh 462033, India (e-mail: piyush@rgtu.net).
Partha Sarkar is with the Department of Electronics and Communication Engineering, National Institute of Technology Durgapur, Durgapur, West Bengal 713209, India (e-mail: parthasarkar.info@gmail.com).
Shweta Singh is with the Department of Electronics and Communication, IES College of Technology, Bhopal 462044, India (e-mail: pariharshwetasingh90@gmail.com).
Ismail Keshta is with the Department of Computer Science and Information Systems, College of Applied Sciences, AlMaarefa University, Riyadh 13713, Saudi Arabia (e-mail: imohamed@mcst.edu.sa).
Ali Rizwan is with the Department of Industrial Engineering, Faculty of Engineering, King Abdulaziz University, Jeddah 21589, Saudi Arabia (e-mail: arkhan71@kau.edu.sa).
Digital Object Identifier 10.1109/TCSS.2022.3213507

I. INTRODUCTION

HYPERTENSION is a long-term medical disease and a major risk factor for other major diseases (e.g., stroke, coronary heart disease, renal failure, and so on) [1]. Its symptoms include flame-shaped hemorrhages at the disk margin, blurred disk margins, congested retinal veins, papilledema, and secondary macular exudates. The disease affects 16%–37% of the global population, and in 2010, high blood pressure was considered to be responsible for 18% of all deaths, so the prevention and treatment of high blood pressure is particularly important. Medical research [2], [3] believes that the use of ophthalmoscopes to detect hypertensive retinopathy (HR) is a part of the evaluation criteria for hypertensive patients. Fundus detection can early detect hypertensive diseases and achieve the purpose of prevention and treatment of hypertension. However, the detection of HR is time-consuming and labor- intensive, so it is necessary to develop an HR detection system
in early screening to improve medical outcomes.

HR is retinal vascular damage caused by hypertension. According to the HR classification proposed in 2004 [4], HR is divided into three grades: mild, moderate, and severe. The symptoms corresponding to mild are generalized stenosis of arterioles, arterial and venous crossing compression, and widening. Enhancement of central light reflex of arterioles; moderately, microaneurysms, retinal hemorrhages, hard exu- dates, and cotton wool appear on the basis of mild symptoms such as macular exudation, severe optic disk edema symptoms, as demonstrated in Fig. 1.

Among them, Fig. 1(a) represents mild HR, the black arrow below represents arterial and venous crossing compression, and the white arrow represents the symptom of arterial copper wire formation. Fig. 1(b) represents moderate HR, the white arrow represents cotton wool spots, and the black arrow rep- resents severe arterial and venous cross compression. Fig. 1(c) shows severe HR, white arrows represent many cotton wool spots, black arrows represent retinal hemorrhages, and black rectangles represent optic disk edema.

According to studies, HR lesions are not well character- ized, and it is difficult to grade them with the naked eye;

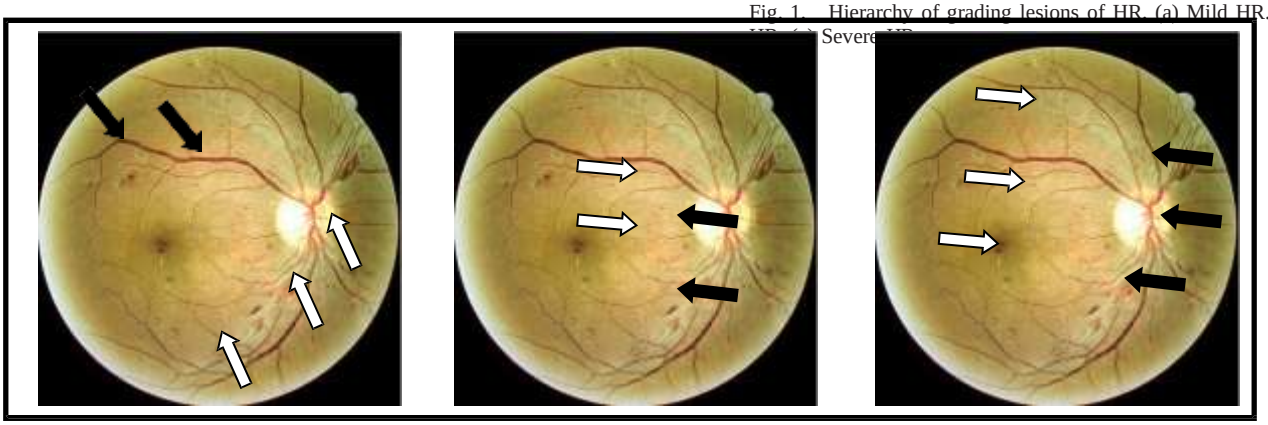

Fig. 1. Hierarchy of grading lesions of HR. (a) Mild HR. (b) Moderate HR. (c) Severe HR.

moderate-to-severe HR is uncommon, with few case samples. Zhang et al. [4] used the Radon vessel tracking algorithm to obtain different feature vectors to classify arteries and veins and then calculated the artery vein ratio (AVR) to achieve HR detection.

Wu et al. [5] proposed using new feature vectors and mixed classification. The AVR algorithm is used to classify the arteries and veins, and the width of the blood vessels is calculated to obtain the AVR to recognize and detect HR.

Most of the previous studies were to identify and detect HR by calculating AVR and did not follow the characteristics of other lesions. Therefore, the identification was based on a sin- gle basis. Inspired by the two-stage 3-D detection algorithm of pulmonary nodules proposed by Liu et al. [7], the local feature classification model and the overall classification model were combined and applied to HR classification. After consulting Sarker et al. [8] and communicating with clinicians, it was concluded that the visible arterial and venous nicking (AVN) lesion feature could represent the severity of HR, so AVN clas- sification is chosen as the local feature classification model.

When a vein is compressed by an artery and assumes a fusion form shape, this pattern is called an AVN. AVN is not only related to current blood pressure, but also to past blood pressure, which indicates that it is an evaluation index of long-term hypertensive disease, so the detection and classification of AVN is a worthy research direction. Aurangzeb et al. [9] used a random forest classifier to classify the width of each part of the vein near the arterial and venous intersection to achieve the purpose of AVN severity classification. Qiao et al. [10] extracted two vein segments and calculated the width of the two vein segments to detect AVN. Hua et al. [13] used algorithms such as vessel segmentation, vessel refinement, and feature point recognition to achieve automatic AVN feature extraction, and complete AVN detec- tion and identification.

From the previous research, there are too many AVN detec- tion and classification based on machine learning, and deep learning is rarely used. In fact, deep learning has certain advan- tages in lesion detection. Li et al. [12] performed lesion detec- tion on diabetic fundus images by improving the R-FCN [13] structure; Niu et al. [14] used the improved GoogleNet [15] neural network, combined with transfer learning to identify and detect liver cirrhosis. Through analysis, it is found that due to the small features of AVN lesions, the common deep learning target detection framework (Faster-RCNN [16], etc.) cannot accurately identify and detect. Therefore, the ROI extraction from the area near the intersection is used for classification, which can solve the problem that the features of the lesions are small and difficult to identify and detect the problem. In terms of extracting intersections, the SeqNet network [17] is used to segment the blood vessels and classify the arteries and veins of the fundus images, and then perform the logical AND operation on the classified arteries and veins to obtain the positions of all intersections in the retinal images. Compared with traditional machine learning, the accuracy of intersection identification and detection is improved.

The motivation and aim to conduct this research are to propose a model for the classification of HR using regional feature fusion. The process is divided into two stages:

1) First, the HR classification can be enhanced by com- bining the features of the local AVN classification model and the overall HR classification model. The goal of Image preprocessing is performed on both models.

In the AVN classification stage, regional AVN image blocks are extracted from the HR image through algorithms, such as blood vessel segmentation, arterial and venous classification, intersection monitoring, and region of interest extraction from the HR original image. The local AVN image block is sent to the improved SeqNet as a new dataset for classification; in the HR classification stage, the preprocessed fundus image is directly sent to the neural network for variety, and finally, the features of the two models are fused as a neural network. The input of the network can improve the HR classification effect. The model is evaluated on a private dataset and compared with other methods to verify the impact of our model.

The AVN classification model's local lesion characteristics and the IoT-FHR classification model's global lesion character- istics were combined using feature mean. After that, the results of the global IoT-FHR classification model are averaged with the results of the local AVN classification model. An easy

neural network receives its input from the final outcome. The probability value of IoT-FHR in the fundus image is output by the sigmoid classifier after the neural network's two fully connected and one dropout layer.

2) A new method for detecting arterial and venous junctions is proposed. Based on the SeqNet network model, logic rules are added to perform logical AND operations on the classified arteries and veins, and the position of the arterial and venous junctions can be obtained. The algorithm is evaluated on the set and compared with the existing research, verifying that the method in this article is effective.

II. FEDERATED LEARNING

Federated learning [1] is a collaborative machine learning framework. The nodes participating in the collaboration use local data to train the model and achieve the prediction effect of multi-source data through parameter aggregation. Artificial intelligence still faces the dilemma of insufficient data sources in the practice process. It takes 10 000 people up to ten years to collect valid data in the medical field [2]. In federated learning, data is stored locally on the node to realize distributed machine learning and collaboration with privacy protection. With the rise of mobile communication technology and intelligent edge devices, federated learning has broad application prospects in the fields of the smart city [3], electronic medical treatment [4], wireless communication [5], and mobile edge network [6] and other fields [7]. Currently, federated learning has produced horizontal federated learning based on data in the same industry, as well as vertical federated learning and federated transfer learning for multi-industry data [8]. Integration has become a research hotspot of common concern in the industry-university-research community.

III. REGIONAL FEATURE FUSION MODEL

The framework of this article is divided into two independent neural networks: the AVN classification model and the HR classification model. The specific frame diagram is shown in Fig. 2.

The input fundus images are sent to two models for classification after image preprocessing. The process of AVN classification is first to use the SeqNet network to perform blood vessel segmentation and arterial and venous classification on the fundus image, second to segment the blood vessels and classify the arteries and veins, and then add a logical AND operation to find the intersection of arteries and veins and perform ROI on the area near the corner. Next, the region of interest is extracted, and finally, the extracted image blocks are sent to the improved ResNet50 [18] neural network for AVN classification; the process of HR classification is to directly send the image to the VGG19 [19], [20], [21] neural network for variety, and finally by averaging the two output of the model is fused to achieve HR classification.

A. AVN Classification Model

As one of the modules of the two-stage model in this article, the AVN classification model includes six parts, namely preprocessing of the input image, blood vessel segmentation, arte- rial and venous classification, arterial and venous intersection

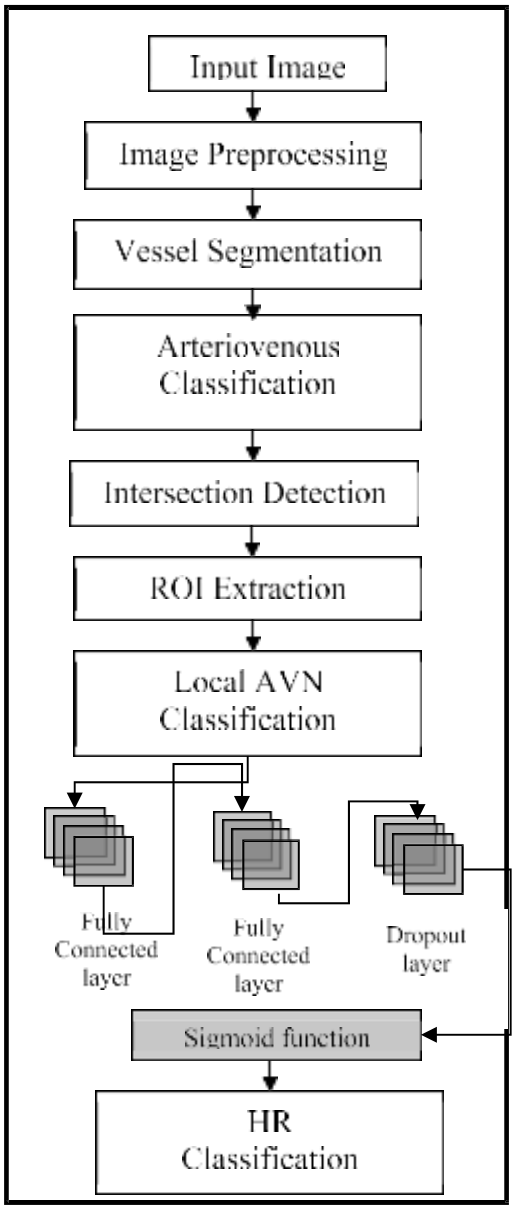

Fig. 2. Model framework.

detection, ROI extraction, and finally, sending the proposed image block into convolutional neural network model for classification, as shown in Fig. 2.

1) Image Preprocessing: Image preprocessing can improve the image's contrast, enhance the intensity of the information of interest, and play an important role in image recognition, detection, and segmentation. The dataset used in this experi- ment is the fundus image data provided by the local hospital. Image preprocessing includes removing black borders, adjust- ing image resolution, data normalization, and augmentation. To remove the black frame, traverse the image pixels, find at least one pixel larger than the set black area threshold, and then extract the adequate border through the broadcast index,

as shown in Fig. 3(a). For subsequent network requirements, choose to adjust the image resolution to 576 × 576. Data normalization adopts the method of subtracting the local

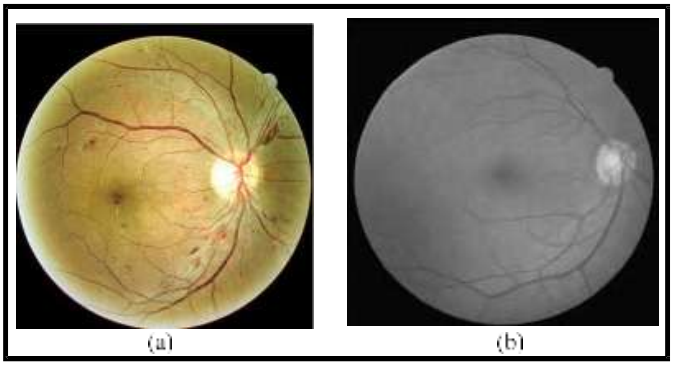

Fig. 3. Preprocessed IoT-FHR fundus renderings image. (a) Original image.
(b) Preprocessed image.

mean [10], and the calculation steps are shown in the following equation:

$$i_{out} = \phi * \beta_{in} + \gamma * i_{gaussian} + \varepsilon. \quad (1)$$

Among them, $\phi = 4$, $\gamma = -4$, $\varepsilon = 128$, i_{out} is the output image, β_{in} is the input image, $i_{gaussian}$ is the image obtained after the input image is processed by Gaussian filtering. The normalization effect is shown in Fig. 3(b). Due to insufficient data, the training effect has a great influence, so rotation, mirroring, and scaling via horizontal and vertical cutting methods are used for data augmentation.

2) Vessel Segmentation and Arterial and Venous Classifi- cation: Retinal vascular extraction and arterial and venous classification play a significant role in detecting various dis- eases. Vessel segmentation and arterial and vein classification are essential steps in AVN detection. For vessel segmentation, Kishor et al. [11] proposed a vessel segmentation model based on a dense attention network, which combined the attention mechanism with a dense connection network to fully extract features to improve the segmentation accuracy of retinal blood vessels; for the classification of arteries and veins, the previous studies used the Radon vessel tracking algorithm to classify the arteries and veins. However, previous works have studied the above two types of tasks separately, without an overall model. This article adopts the SeqNet model proposed by Qiao et al. [10], which can perform blood vessel segmentation and arterial and venous classification at the same time. The model has been described in detail in the literature [12]. This section briefly introduces the algorithm principle of the model. SeqNet comprises two parts, and the first adopts IterNet [12] complete vessel segmentation. IterNet is composed of multiple iterations of a small U-net [13]. Its depth is four times larger than an ordinary U-net, and it can learn only from a small number of labels without pre-training and prior knowledge. The effect of blood vessel segmentation is shown in Fig. 4(a). The second part uses a U-net of another size to complete the arterial and vein classification and masks the background pixels in the input image, as shown in (2) as follows:

$$i_{out} = i_{in} * v_{image}. \quad (2)$$

Among them, i_{out} is the masked image, i_{in} is the original retinal image, and v_{image} is the refined blood vessel image. Multiplying the original retinal image and the refined blood vessel image element by element can reduce the complexity of the input image so that the classification network can entirely focus on finding differences in the blood vessels' color, shape, thickness, etc. The effect diagram is shown in Fig. 4(b), and the specific network structure is shown in Fig. 5. This article uses the DRIVE [24], LES_AV[25], and HRF[26] datasets to train the SeqNet network and applies the trained model to the IoT-FHR dataset for vessel segmentation and arterial and vein classification.

3) Arterial and Venous Junction Detection: The vascular structure is mainly composed of bifurcation and intersection. A bifurcation is splitting a blood vessel into two blood vessels, and the bifurcation point is the position where the blood vessel splits. The intersection is the intersection of two blood vessels (arteries and veins), and the intersection is the position where the blood vessels cross, as shown in Fig. 6.

AVN is known to occur at the location of arterial and venous intersections, so it is first necessary to detect all intersections within the retinal fundus image. This article adds logic rules based on the SeqNet network structure, and the classified arteries and veins are logically AND ed. The specific network model is shown in Fig. 6.

It can be seen from Fig. 6 that SeqNet outputs the classification vectors of arteries and veins after classifying the arteries and veins. Due to the known prior knowledge, the intersection of arteries and veins is the intersection of arteries and veins. Therefore, this article formulates a logical rule AND operation to perform logical AND operation on the output vectors of arteries and veins and finally obtain a vector. AND operation basically reflects the presence of arteries and veins on the final output vector, whereas OR only shows the presence of anyone. This vector maps back to the figure where the arterial and venous classification use the specific calculation method shown in the following equation:

$$a \cap b = c. \quad (3)$$

Among them, a represents the vector of the classified artery, b represents the vector of the classified vein, $\wedge$ rep- resents the logical AND operation, and c represents the vector obtained after the AND operation of the arterial and venous classification.

Equation (3) derived a logical rule AND operation to perform a logical AND operation on the output vectors of arteries and veins, resulting in a vector. The AND operation reflects the presence of arteries and veins on the final output vector, whereas the OR operation shows the presence of anyone.

4) ROI Extraction: Analyzing the hospital dataset shows that the size of AVN lesions is generally distributed between 30 and 40 pixels, and the traditional target detection algorithm cannot accurately detect and classify them. The size is set to 224 × 224 pixels, and the image patches are filtered to ensure each image patch has an intersection.

B. IoT-FHR Classification Model

The IoT-FHR classification model, another model in the two-stage model in this article, preprocesses the input fundus

Fig. 4. Segmentation, arterial and venous classification. (a) Vessel segmentation. (b) Arterial and venous classification.

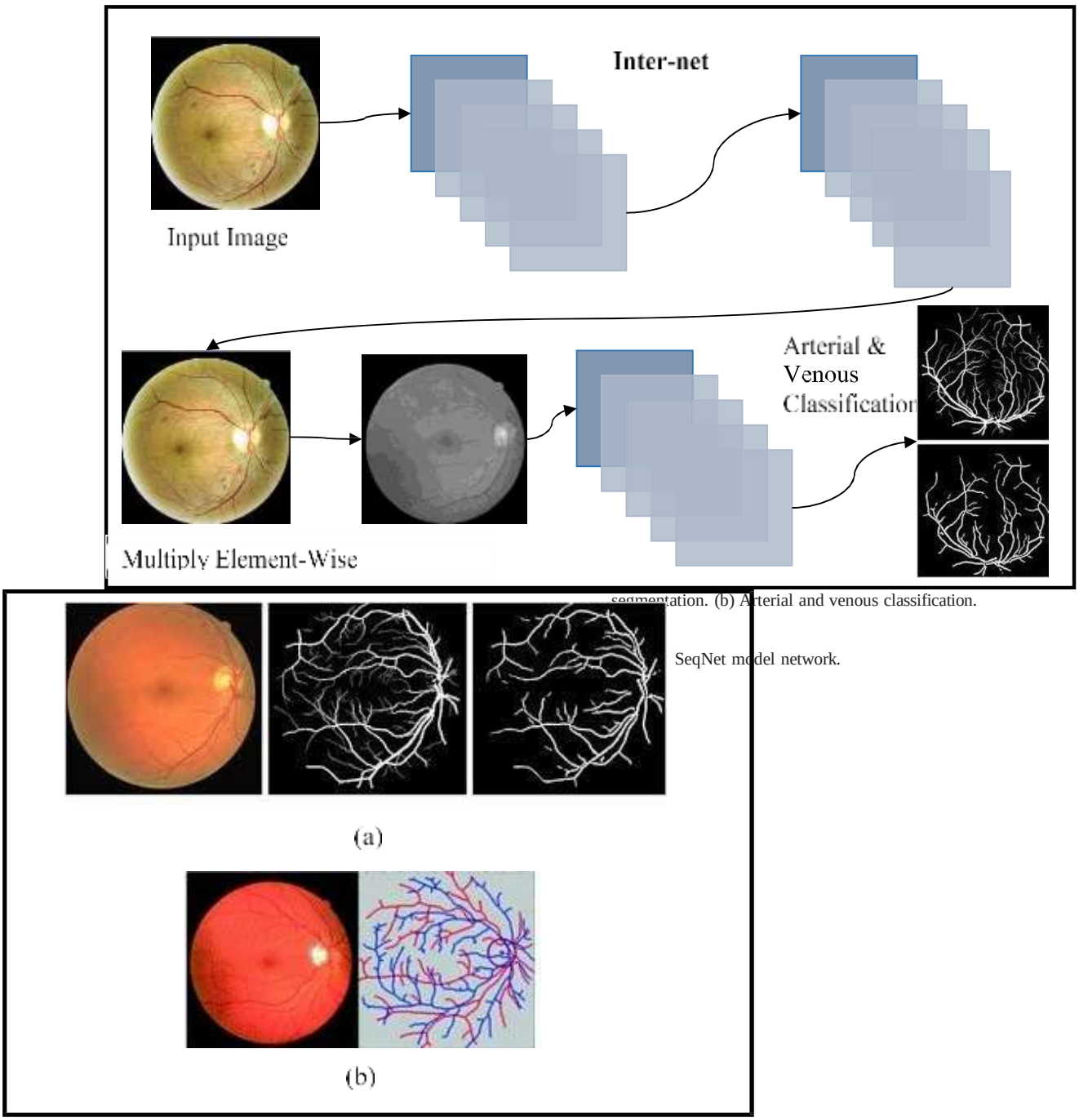

SeqNet model network.

image through the algorithm proposed and directly sends the preprocessed image to the VGG19 network for classification. The optimizer is set to the SGD optimizer, the learning rate is 0.001, the loss function is binary_crossentropy cross-entropy loss function, and the classifier is sigmoid.

C. Model Fusion

The global lesion characteristics of the IoT-FHR classification model and the local lesion characteristics of the AVN classification model were summed by feature mean. Next, the output of the local AVN classification model is weighted and averaged with the output of the overall IoT-FHR classification model. The final result is used as the input of a simple neural network. The neural network consists of two fully connected layers and a dropout layer, and finally, the sigmoid classifier outputs the probability value of IoT-FHR in the fundus image.

IV. Experimental Setup and Result Analysis

The experimental environment of this article is done on python which used the Keras library with Tensorflow as the

Fig. 6. Improved SeqNet intersection detection framework.

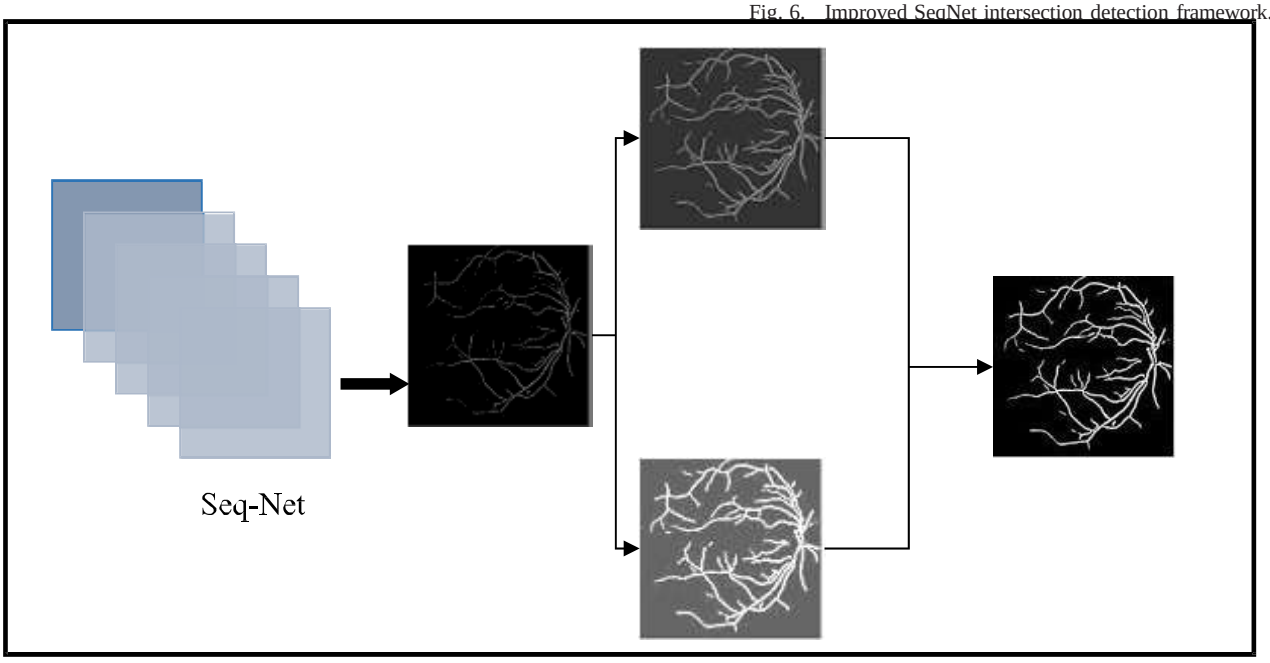

backend. Source framework, the corresponding versions are Tensorflow1.15.0 and Keras2.3.1. GPU.

A. Dataset

The dataset used in this experiment is the fundus image dataset provided by the local hospital, including 48 IoT-FHR fundus images and 48 standard fundus images, each with a resolution of 2592 × 1728. Among them, the data for mild and moderate hypertension are less, and the fundus data for severe
hypertension are more. The reason for the analysis is that because the early symptoms of hypertension are not obvious, the patients who undergo physical examination rarely undergo fundus screening. In addition, it was found that the age of the dataset was widely distributed between 50 and 70 years old, and most of the patients were male. The two types of models use different datasets, respectively. The dataset used by the IoT-FHR classification model is 1276 IoT-FHR fundus images after data augmentation, including 1012 training sets and 264 testing sets. The fundus image is marked as the existence of IoT-FHR fundus and normal fundus; the dataset used by the AVN classification model is the regional image set extracted from the IoT-FHR classification model dataset through the ROI in Section III, a total of 124 images, after data expansion. After the increase, there are 1364 image blocks, including 1090 in the training set and 274 in the test set. The datasets were annotated by ophthalmologists and marked as 0 and 3, representing no AVN and the presence of AVN (including mild AVN, moderate AVN, and severe AVN), respectively.

B. Model Performance Analysis

In this article, three evaluation indicators, accuracy (ACC), sensitivity (SENS), and specificity (SPEC), are used to evaluate the performance of the proposed method. ACC is the identification rate of correct classification of detected lesions; SENS is also known as the true positive rate, that is, the probability that it has the characteristics of the lesion and is diagnosed as diseased, which is the standard to measure the correct judgment of the fundus image lesions in this article; SPEC is also called the true negative rate, that is, the probability of actually not having the disease and being diagnosed as having no disease, as shown in the following
equations:

$$Acc = \frac{TP}{TP + TN + FP + FN} + TN \quad (4)$$

$$Sens = \frac{TP}{TP + FN} \quad (5)$$

$$Spec = \frac{TN}{TN + FP} . \quad (6)$$

Among them, TP means that the method in this article correctly identifies the fundus image with the actual characteristics of the lesion, FP means that this article recognizes the actual normal fundus image as the lesion image, and FN means that this article incorrectly identifies the actual diseased fundus image as the normal fundus image, and TN means the actual normal fundus image is correctly identified.

1) Classification Performance of Proposed Model: To illus- trate the classification performance of the improved ResNet50 network based on the dataset in this article, the original ResNet50 is compared with the enhanced model. The dataset used the AVN dataset, and the evaluation indicators are the training set (train_acc) and the accuracy of the test set (test_acc), as shown in Table I.

As can be seen from Table I, the accuracy of the original ResNet network training set is high, but the accuracy of the test set is not high. By analyzing the data and model, we know

TABLE I
CLASSIFICATION PERFORMANCE OF PROPOSED MODEL

Model	Train_Acc	Test_Acc
ResNet	88.69	79.56
IoT-FHR	89.56	86.45

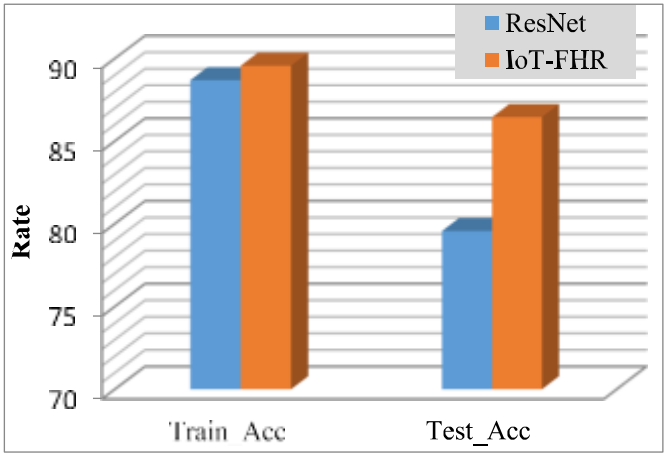

Fig. 7. Classification performance of proposed model.

TABLE II
CLASSIFICATION PERFORMANCE OF PROPOSED MODEL OVER DIFFERENT PIXEL

ROI/bit	Accuracy	Sensitivity	Specificity
656*656	74.56	65.24	76.58
284*284	89.56	68.96	92.89
180*180	86.54	68.21	90.58
70*70	79.28	62.48	81.28

that this is because the dataset in this article is small and noisy, and the training model is prone to overfitting.

Therefore, this article improves the original network, changes the original flattened layer to the global average pooling 2-D layer, adds a dense connection layer, and adds L2 regularization and batch norm to reduce overfitting. Compared with the experimental results, it is found that the improved model has a better classification effect on the dataset in this article, as shown in Fig. 7.

2) Classification Performance of Proposed Model Over Different Pixel: To explore the influence of the size of the selected area on the AVN classification model in this article, multiple areas will be chosen for AVN classification, as shown in Table II.

It can be seen from Table II that when the ROI size is selected as 284 × 284, the model accuracy, sensitivity, and specificity results are the highest. On the other hand, it can be seen from the table that when there are multiple intersections

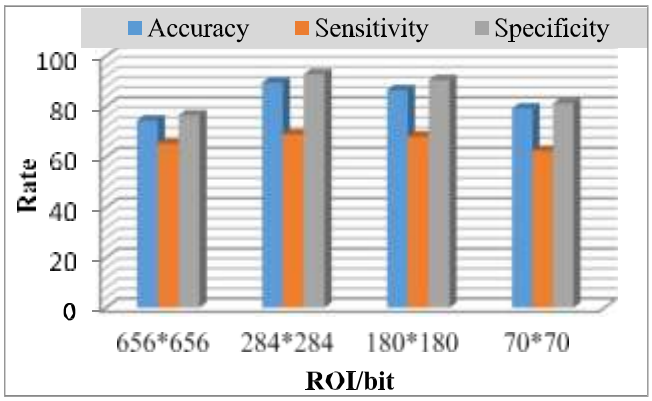

Fig. 8. Classification performance of proposed model over different pixels.

TABLE III
CLASSIFICATION PERFORMANCE OF PROPOSED MODEL WITH EXISTING MODEL

ROI/bit	Accuracy	Sensitivity	Specificity
	64.87	56.76	66.62
Modified PSO [9]	77.92	60.00	80.81
Vessel Parameters [10]	68.97	54.36	70.71
IoT-FHR			

in each image, when the area size is 656 × 656, the network classification performance is not good.

The reason for the analysis is that when the image features are reduced, the features of the intersections become small and difficult to identify, as shown in Fig. 8. It makes the neural network unable to distinguish whether the fundus image has AVN accurately, and when the area size is 70 × 70, the network classification performance is not very good. The reason is that when the image features are enlarged to a certain extent, the blood vessel features may be distorted and blurred. The neural network is still unable to identify the situation accurately. Therefore, it can be concluded that the selection of image blocks with different area sizes has a particular impact on AVN classification. Experiments have proved that the model effect is the best when the area size is 284 × 284. To illustrate the efficiency of the AVN classification model used in this article, the way this article is compared with the representative AVN classification methods in recent years and the experimental results are shown in Table III.

The data in Fig. 9 shows that the model proposed in this research has a specific improvement in accuracy and sensitivity to other methods, and the specificity is slightly lower than other methods. In the medical field, high sensitivity represents a low rate of missed diagnosis, and high specificity means a low rate of misdiagnosis.

3) Classification Performance of Proposed Model With Existing Model: Since the AVN classification designates the severity of HR, a model with high specificity and high sensitivity can effectively identify whether the fundus image is a

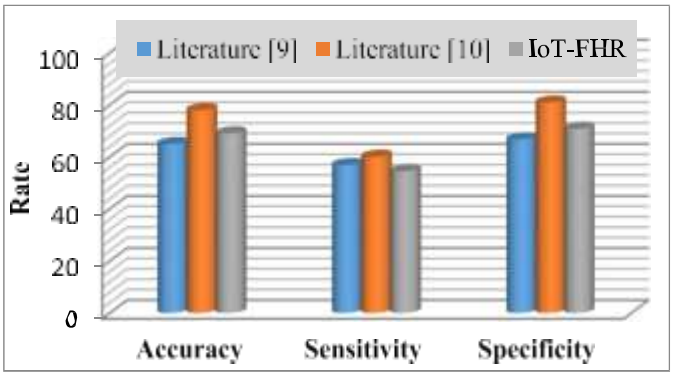

Fig. 9. Classification performance of proposed model with existing model.

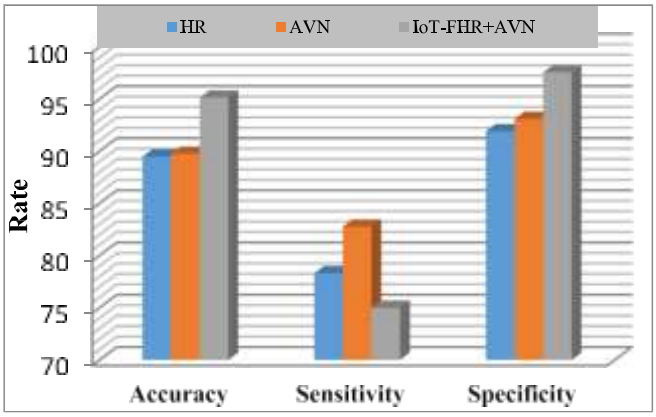

Fig. 10. Classification performance of proposed model over different AVN classifications.

TABLE IV
CLASSIFICATION PERFORMANCE OF PROPOSED MODEL OVER DIFFERENT AVN CLASSIFICATION

ROI/bit	Accuracy	Sensitivity	Specificity
HR	89.47	78.29	91.90
AVN	89.74	82.75	93.08
IoT-FHR+AVN	95.14	74.98	97.54

feature of AVN lesions and infer the severity of IoT-FHR in this patient. According to the above analysis, this method has significant advantages compared with other methods.

To verify the performance of the two-stage IoT-FHR classification model proposed in this article, the proposed method is compared with the single-stage VGG19-based IoT-FHR fundus image classification method and the ResNet50-based AVN classification method. The experimental comparison results are shown in Table IV.

From the data in Table IV, it can be seen that an accuracy of 89.47% can be obtained by directly sending the preprocessed IoT-FHR images into the neural network, indicating that the neural network can identify the characteristics of IoT-FHR lesions. Still, the classification effect is not good enough. The AVN classification algorithm alone shows an accuracy of 89.74%, indicating that the network is sensitive to local features. The research conducted in this article to fuse global and local components achieves an accuracy of 95.14%, a sensitivity of 74.98%, and a specificity of 97.54%. It shows that the model fusion algorithm can enhance the characteristics of lesions and improve the classification performance of HR. The method in this article is superior to the single-stage IoT-FHR fundus image classification in accuracy, sensitivity, and specificity, indicating that adding the AVN classification model for feature fusion can effectively increase the overall IoT-FHR classification effect, as shown in Fig. 10.

The model in this article classifies all six images correctly, and the classification results are two IoT-FHR fundus images and four normal fundus images. It can be proved that the model in this article can not only identify the hypertension dataset of the local hospital but also identify whether other fundus images have HR, indicating that the model has specific generalization and robustness.

V. CONCLUSION

This article proposes an IoT-FHR classification model based on regional feature fusion. The proposed model is classified into two sections: the IoT-FHR classification model and the AVN classification model. For these two models, the IoT-FHR fundus images are preprocessed by removing black borders, subtracting local mean values, and data augmentation to obtain preprocessed images. The IoT-FHR classification model sends the preprocessed fundus images directly to the VGG19 net- work for classification; the AVN classification model sends the images to the SeqNet network for blood vessel segmentation and arterial and venous classification and uses the intersection detection method to detect all arteries and veins in the image. Intersection, extract the image blocks in the area near the meeting and send the extracted image blocks to the improved ResNet50 network for classification. Finally, the weighted average of the two features is sent to a simple neural network as a whole for classification. This article supports visualization in each process step to ensure the intuitiveness of the model effect. The efficiency of the model is assessed in terms of accuracy, sensitivity, and specificity and then it is compared with previously implemented methods. It can be seen from the experimental results that the classification of regional feature fusion can provide better results. The method proposed in this article to fuse global and local components achieves an accuracy of 95.14%, a sensitivity of 74.98%, and a specificity of 97.54%.

Future methods will use an advanced model fusion algorithm to fuse the two models to improve the classification effect of the model.

REFERENCES

[1] H. Elayan, M. Aloqaily, and M. Guizani, "Sustainability of healthcare data analysis IoT-based systems using deep federated learning," *IEEE Internet Things J.*, vol. 9, no. 10, pp. 7338–7346, May 2022, doi: 10.1109/JIOT.2021.3103635.

[2] S. Zhai, X. Jin, L. Wei, H. Luo, and M. Cao, "Dynamic federated learning for GMEC with time-varying wireless link," *IEEE Access*, vol. 9, pp. 10400–10412, 2021, doi: 10.1109/ACCESS.2021.3050172.

[3] C. Chakraborty, A. Kishor, and J. J. P. C. Rodrigues, "Novel enhanced- grey wolf optimization hybrid machine learning technique for bio- medical data computation," *Comput. Electr. Eng.*, vol. 99, Apr. 2022, Art. no. 107778.

[4] C. Zhang, L. Cui, S. Yu, and J. J. Q. Yu, "A communication-efficient federated learning scheme for IoT-based traffic forecasting," *IEEE Internet Things J.*, vol. 9, no. 14, pp. 11918–11931, Jul. 2022, doi: 10.1109/JIOT.2021.3132363.

[5] Q. Wu, K. He, and X. Chen, "Personalized federated learn- ing for intelligent IoT applications: A cloud-edge based frame-work," *IEEE Open J. Comput. Soc.*, vol. 1, pp. 35–44, 2020, doi: 10.1109/OJCS.2020.2993259.

[6] R. Xu and Y. Chen, "μDFL: A secure microchained decentralized federated learning fabric atop IoT networks," *IEEE Trans. Network Service Manag.*, vol. 19, no. 3, pp. 2677–2688, Sep. 2022, doi: 10.1109/TNSM.2022.3179892.

[7] W. Liu et al., "Intrusion detection for maritime transportation systems with batch federated aggregation," *IEEE Trans. Intell. Transp. Syst.*, early access, Jun. 14, 2022, doi: 10.1109/TITS.2022.3181436.

[8] P. S. Sarker, S. K. Sadanandan, and A. K. Srivastava, "Resiliency metrics for monitoring and analysis of cyber-power distribution system with IoTs," *IEEE Internet Things J.*, early access, Jun. 14, 2022, doi: 10.1109/JIOT.2022.3183180.

[9] K. Aurangzeb, S. Aslam, M. Alhussein, R. A. Naqvi, M. Arsalan, and S. I. Haider, "Contrast enhancement of fundus images by employ- ing modified PSO for improving the performance of deep learn- ing models," *IEEE Access*, vol. 9, pp. 47930–47945, 2021, doi: 10.1109/ACCESS.2021.3068477.

[10] L. Qiao, Y. Zhu, and H. Zhou, "Diabetic retinopathy detection using prognosis of microaneurysm and early diagnosis system for non-proliferative diabetic retinopathy based on deep learning algorithms," *IEEE Access*, vol. 8, pp. 104292–104302, 2020, doi: 10.1109/ACCESS.2020.2993937.

[11] A. Kishor, C. Chakraborty, and W. Jeberson, "Reinforcement learning for medical information processing over heterogeneous networks," *Multimedia Tools Appl.*, vol. 80 pp. 23983–24004, Mar. 2021.

[12] X. Li, X. Hu, L. Yu, L. Zhu, C.-W. Fu, and P.-A. Heng, "CANet: Cross- disease attention network for joint diabetic retinopathy and diabetic macular edema grading," *IEEE Trans. Med. Imag.*, vol. 39, no. 5, pp. 1483–1493, Nov. 2020, doi: 10.1109/TMI.2019.2951844.

[13] C.-H. Hua et al., "Convolutional network with twofold feature augmen- tation for diabetic retinopathy recognition from multi-modal images," *IEEE J. Biomed. Health Informat.*, vol. 25, no. 7, pp. 2686–2697, Jul. 2021, doi: 10.1109/JBHI.2020.3041848.

[14] Y. Niu, L. Gu, Y. Zhao, and F. Lu, "Explainable diabetic retinopathy detection and retinal image generation," *IEEE J. Bio- med. Health Informat.*, vol. 26, no. 1, pp. 44–55, Jan. 2022, doi: 10.1109/JBHI.2021.3110593.

[15] A. Kishor and C. Chakraborty, "Artificial intelligence and Internet of Things based healthcare 4.0 monitoring system," *Wireless Pers. Commun.*, 2021, doi: 10.1007/s11277-021-08708-5.

[16] M. M. Abdelsalam and M. A. Zahran, "A novel approach of diabetic retinopathy early detection based on multifractal geometry analysis for OCTA macular images using support vector machine," *IEEE Access*, vol. 9, pp. 22844–22858, 2021, doi: 10.1109/ACCESS.2021.3054743.

[17] J. Wang, Y. Bai, and B. Xia, "Simultaneous diagnosis of severity and features of diabetic retinopathy in fundus photography using deep learn-ing," *IEEE J. Biomed. Health Informat.*, vol. 24, no. 12, pp. 3397–3407, Dec. 2020, doi: 10.1109/JBHI.2020.3012547.

[18] Y. Peng et al., "Automatic staging for retinopathy of prematurity with deep feature fusion and ordinal classification strategy," *IEEE Trans. Med. Imag.*, vol. 40, no. 7, pp. 1750–1762, Jul. 2021, doi: 10.1109/TMI.2021.3065753.

[19] M. Niemeijer et al., "Automated measurement of the arteriolar- to-venular width ratio in digital color fundus photographs," *IEEE Trans. Med. Imag.*, vol. 30, no. 11, pp. 1941–1950, Nov. 2011, doi: 10.1109/TMI.2011.2159619.

[20] Y. Zhao et al., "Intensity and compactness enabled saliency esti- mation for leakage detection in diabetic and malarial retinopathy," *IEEE Trans. Med. Imag.*, vol. 36, no. 1, pp. 51–63, Jan. 2017, doi: 10.1109/TMI.2016.2593725.

[21] S. Qummar et al., "A deep learning ensemble approach for diabetic retinopathy detection," *IEEE Access*, vol. 7, pp. 150530–150539, 2019, doi: 10.1109/ACCESS.2019.2947484.